ELSEVIER

NeuroImage

www.elsevier.com/locate/ynimg
NeuroImage 41 (2008) 1199–1205

$T1_\rho$ MRI of Alzheimer's disease

Arijitt Borthakur,[a,*] Matthew Sochor,[a] Christos Davatzikos,[b] John Q. Trojanowski,[c] and Christopher M. Clark[d]

[a]*MMRRCC, Department of Radiology, University of Pennsylvania, Philadelphia, PA, USA*
[b]*SBIA, Department of Radiology, University of Pennsylvania, Philadelphia, PA, USA*
[c]*Center for Neurodegenerative Disease Research, Department of Pathology and Laboratory Medicine, University of Pennsylvania, Philadelphia, PA, USA*
[d]*Penn Memory Center, Department of Neurology, University of Pennsylvania, Philadelphia, PA, USA*

Received 4 December 2007; revised 28 February 2008; accepted 18 March 2008
Available online 1 April 2008

Alzheimer's disease (AD) is the most common form of dementia in the elderly. Classic symptoms of the disease include memory loss and confusion associated with the hallmark neuro-pathologic lesions of neurofibrillary tangles (NFT) and senile plaques (SP) and their sequelae, gray matter atrophy. Volumetric assessment methods measure tissue atrophy, which typically follows early biochemical changes. An alternate MRI contrast mechanism to visualize the early pathological changes is $T_{1\rho}$ (or "T-1-rho"), the spin lattice relaxation time constant in the rotating frame, which determines the decay of the transverse magnetization in the presence of a "spin-lock" radio-frequency field. Macromolecular changes (in plaques and tangles) that accompany early AD are expected to alter bulk water $T_{1\rho}$ relaxation times. In this work, we measure $T_{1\rho}$ MRI on patients with clinically diagnosed AD, MCI and in age-matched cognitively normal control subjects in order to compare $T_{1\rho}$ values with changes in brain volume in the same regions of the brain and demonstrate that $T_{1\rho}$ can potentially constitute an important biomarker of AD.

Keywords: T1rho; Spin-lock imaging; Alzheimer's disease

Introduction

Alzheimer's Disease (AD) is the most common form of dementia in the elderly (Dawbarn and Allen, 2001). Classic symptoms of the disease include memory loss, confusion and biological features such as the formation of neurofibrillary tangles (NFT), senile plaques (SP) of amyloid-β protein and gray matter atrophy in the brain (Selkoe, 1999; Lee et al., 2001; Uryu et al., 2002). As early diagnosis (10 years before the onset of neurological symptoms) could provide a more positive outcome and as specific drug therapies are developed, there is an increasing demand for an early and non-invasive diagnosis of AD.

Development of quantitative non-invasive imaging methods of diagnosing AD have resulted in MRI-based methods that rely on contrast generated by the variation of T_1 and T_2 relaxation times of water in tissue. The formation of NFT, SP, resulting cellular loss, and decreased gray matter are expected to change the biochemical environment of the affected brain region. There are situations where structural deformities may not be evident but other clinical diagnoses indicate the impairment of normal brain function. In such cases PET and fMRI techniques provide an alternate method of diagnosis. PET imaging uses radioactive tracers to measure glucose metabolism or blood flow. This technique suffers from poor resolution and wide-scale clinical applicability is hampered by the fact that the imaging center must possess a cyclotron that can produce radioactive tracers. Functional MRI permits the imaging of brain function, without the use of ionizing radiation while the patient is made to perform a cognitive task (Gonzalez et al., 1995; Moseley et al., 1996). But functional imaging has not been able to distinguish between AD and other dementias and has not been established as a diagnostic method for AD.

However, applications of these MRI techniques towards diagnosing AD in its early stages have not yielded conclusive results since clinical MRI resolution (>300 μm pixel size) is inadequate to observe the actual plaques and NFT. For these reasons, volumetric assessment methods are used in current state-of-the-art MRI of AD. Yet even these methods only measure tissue atrophy, subsequent to early biochemical changes.

Detecting changes in the early stages of any degenerative process would help distinguish patterns of atrophy and facilitate differential diagnosis. Regions of interest in the brain include sub-structures of the medial temporal lobe such as the hippocampus, amygdala and entorhinal cortex (Jack et al., 1999; De Santi et al., 2001; Hampel et al., 2002; Chetelat and Baron 2003; de Leon et al.

* Corresponding author. University of Pennsylvania, B1 Stellar-Chance Laboratories, 422 Curie Boulevard, Philadelphia, PA 19104-6100, USA. Fax: +1 215 573 2113.
E-mail address: ari@mail.mmrrcc.upenn.edu (A. Borthakur).
URL: http://www.mmrrcc.upenn.edu (A. Borthakur).
Available online on ScienceDirect (www.sciencedirect.com).

1053-8119/$ - see front matter © 2008 Elsevier Inc. All rights reserved.
doi:10.1016/j.neuroimage.2008.03.030

2006). Early AD is associated with neuronal loss and consequent changes in gray matter, which eventually leads to the atrophy of cortical gyri and widening of sulci. Structural imaging of the brain by MRI helps to differentiate tissue types, identify structural lesions and visualize spatial patterns of atrophy. The quantitative measurement of structural changes is sub-divided into linear, 2D cross-sectional or 3D volumetric analyses, each with its own advantages and shortcomings. With speed and simplicity, linear measurements of inter-object distances in the brain are able to differentiate between normal and AD-affected patients but with significant overlap between normal controls and mild AD-affected individuals (DeCarli et al., 1990). Morphological changes monitored in 2D cross-sections lack the full potential of volumetric analyses but are generally less time-consuming (Cook et al., 1992). The volume of CSF, gray

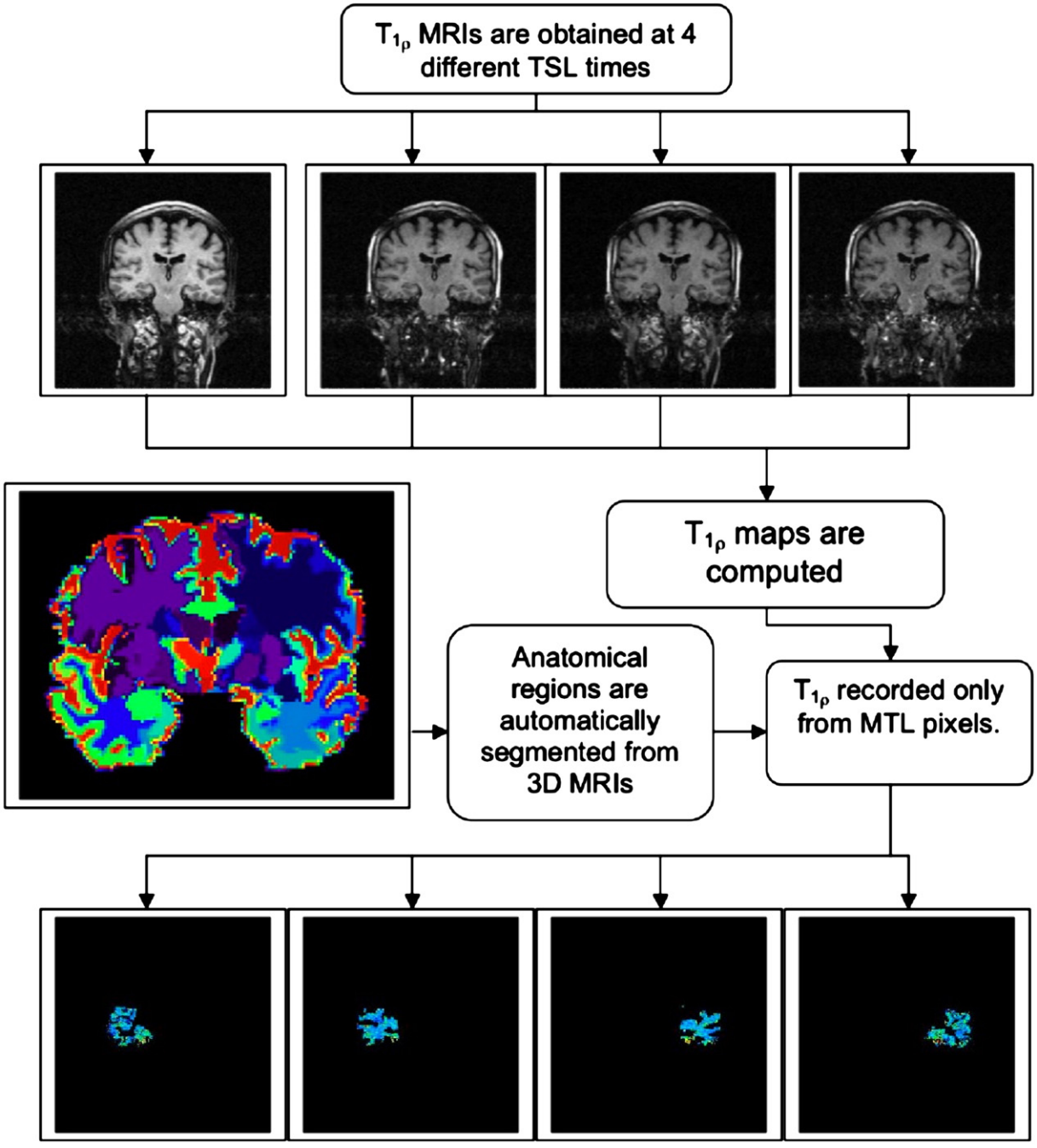

Fig. 1. A flow chart of automated $T_{1\rho}$ data reporting method. $T_{1\rho}$ maps are computed for the entire brain from 4 TSL time images. Atrophy in the brain is determined by using high-dimensional deformable registration methods developed by collaborator Davatzikos (Shen and Davatzikos, 2002). 3D MRI scans of different brains are deformed into a standardized template to generate anatomical maps (a typical slice from a 3D data set is shown in color on the left). Once labeled, these are reformed into the original brain shape. Atrophy rates can then be measured from two time points using these deformation maps (Davatzikos et al., 2001). The labeled template can also be used to report $T_{1\rho}$ values from any region of the brain. As an example, GM and WM pixels from left and right medial temporal lobes are shown as four segmented images at the bottom of the figure.

matter (GM), and white matter (WM) change with the progression of AD (Sullivan et al., 1993; Convit et al., 1997; Thompson et al., 2007). But small and especially focal changes (1–2% decrease in volume) may not be detectable with enough sensitivity to distinguish between normal age-related volume decrease and AD-related changes. Furthermore, volumetric methods require correction for potential brain-size variations present before the onset of AD (Pfefferbaum et al., 1994). Although very high-resolution MRI (<100 μm) has been used to image plaque formations in tissue specimens (Benveniste et al., 1999) and in mice *in vivo* (McDaniel et al., 2001), the required sub-micron resolution of this technique is not attainable on clinical MRI scanners.

MRI provides exquisite soft-tissue contrast provided by the T_1 and T_2 relaxation mechanisms in the different tissues in the brain. For example, tissues with highly mobile water e.g. CSF appear bright in T_2-weighted MR images, whereas brain parenchyma is highlighted in T_1-weighted images. Recent studies have shown that *in vivo* relaxometric measurements of T_2 differ by ~3 ms between transgenic (tg) mice and age-matched controls (Helpern et al., 2004). However, Campeau et al demonstrated that hippocampal T_2 was not significantly different between Alzheimer's disease patients and normal subjects (9). An alternate contrast mechanism is $T_{1\rho}$, or "T-1-rho", the spin lattice relaxation time constant in the rotating frame, which determines the decay of the transverse magnetization in the presence of a "spin-lock" radio-frequency field. $T_{1\rho}$ MRI has previously been used to measure $T_{1\rho}$ relaxation times in normal brains *in vivo* (Borthakur et al., 2004). The $T_{1\rho}$ relaxation time constant is influenced by molecular processes that occur in the millisecond range, such as chemical exchange of protons between water associated with macromolecules and free water. In biological tissues, $T_{1\rho}$ is dependent on the macromolecular composition and provides contrast unlike conventional T_1/T_2-based methods. Further, $T_{1\rho}$ displays a greater range of values compared to T_2 in the human brain (Borthakur et al. 2004). $T_{1\rho}$ contrast has also shown promise in delineating tumors (Markkola et al., 1998), gliomas (Aronen et al., 1999), and other cancerous tissue (Santyr 1994; Dixon et al., 1996).

Recent work by our group has demonstrated the feasibility of measuring plaque burden in the APP/PS1 transgenic mouse model of AD (Borthakur et al., 2006a).

Quantitative $T_{1\rho}$ MRI is, therefore, an attractive proposition for the diagnosis of neuro-degenerative diseases such as AD at clinically-feasible MRI resolution. In this study, we provide valuable baseline values of $T_{1\rho}$ in the brains of normal, MCI and AD-affected patients and determine whether there are any significant differences between these cohorts. These measurements were performed in the medial temporal lobe region of the brain that is primarily associated with AD pathology (DeCarli et al., 1990; Sandor et al., 1992; Jack et al., 2004).

Methods

Preparing for MRI

The Institutional Review Board of the University of Pennsylvania approved all experiments as part of a large ongoing study that will examine 350 AD and MCI patients and controls over the next 2 years. For the results presented here, MRI was performed on only 14 AD patients (mean age 79±2) classified as AD, 11 MCI patients (mean age: 76±2), and 16 elderly controls (mean age: 78±2) on a Siemens Sonata 1.5 Tesla clinical scanner with the vendor-supplied head coil. AD and MCI patients were diagnosed initially by a neurologist (C.M.C.) as such based on their psychiatric history and standard MMSE cognitive testing.

Estimation of $T_{1\rho}$ in the brain

An oblique coronal $T_{1\rho}$-weighted image of a slice perpendicular to the AC/PC plane was obtained. This slice was chosen to include the head of the hippocampus. An inversion pulse-prepared (fluid-attenuated) $T_{1\rho}$ pre-encoded Turbo Spin-Echo (TSE) pulse sequence (Borthakur et al., 2004) was used to acquire all images. Imaging parameters were: TE/TR=12/2000 ms, TSL (duration of spin-lock pulse)=10, 20, 30, 40 ms, with a spin-lock frequency of 500Hz, ms, slice thickness=2 mm, FOV=22 cm, Matrix size=256×128, bandwidth=130 Hz/pixel, echo train length=4 for a total imaging time of 6 min for four images. The time of inversion (TI) was fixed at 860 ms to remove the contribution from CSF to the $T_{1\rho}$ maps, especially in the AD patients that tend to display large sulcal and ventricular CSF. In the initial evaluation of the fluid-attenuated $T_{1\rho}$ MRI protocol, we also obtained $T_{1\rho}$ images and maps from a non-fluid-attenuated $T_{1\rho}$ MRI pulse sequence protocol with identical imaging parameters but without the inversion pulse. Each image pixel's signal intensity was fitted as a function of TSL by a linear least-squares algorithm to generate $T_{1\rho}$ maps (Borthakur et al., 2004).

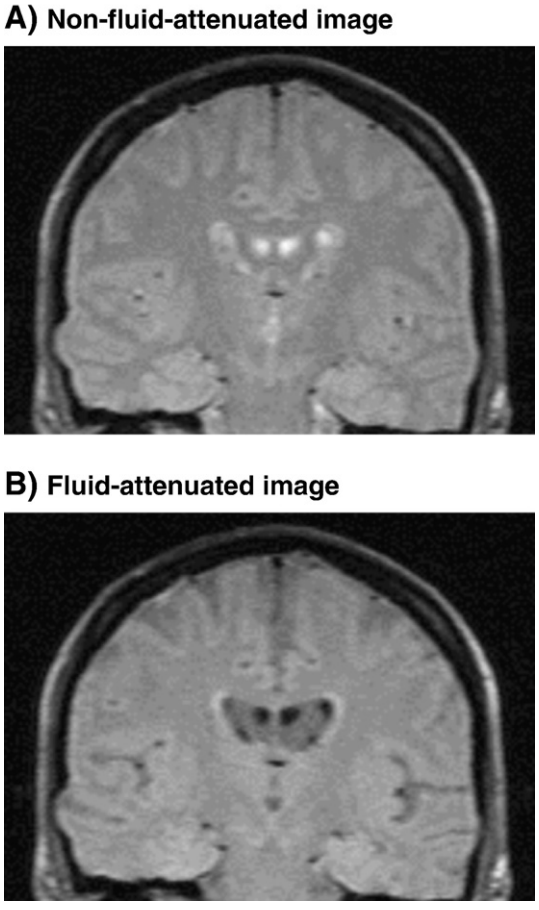

Fig. 2. Conventional $T_{1\rho}$ (A) and fluid-attenuated $T_{1\rho}$ (B) images from the AD patient's brain data are shown. Note the lack of signal from the CSF in the ventricles in figure B. As expected, the SNR of surrounding brain parenchyma was slightly lower in figure B than in A.

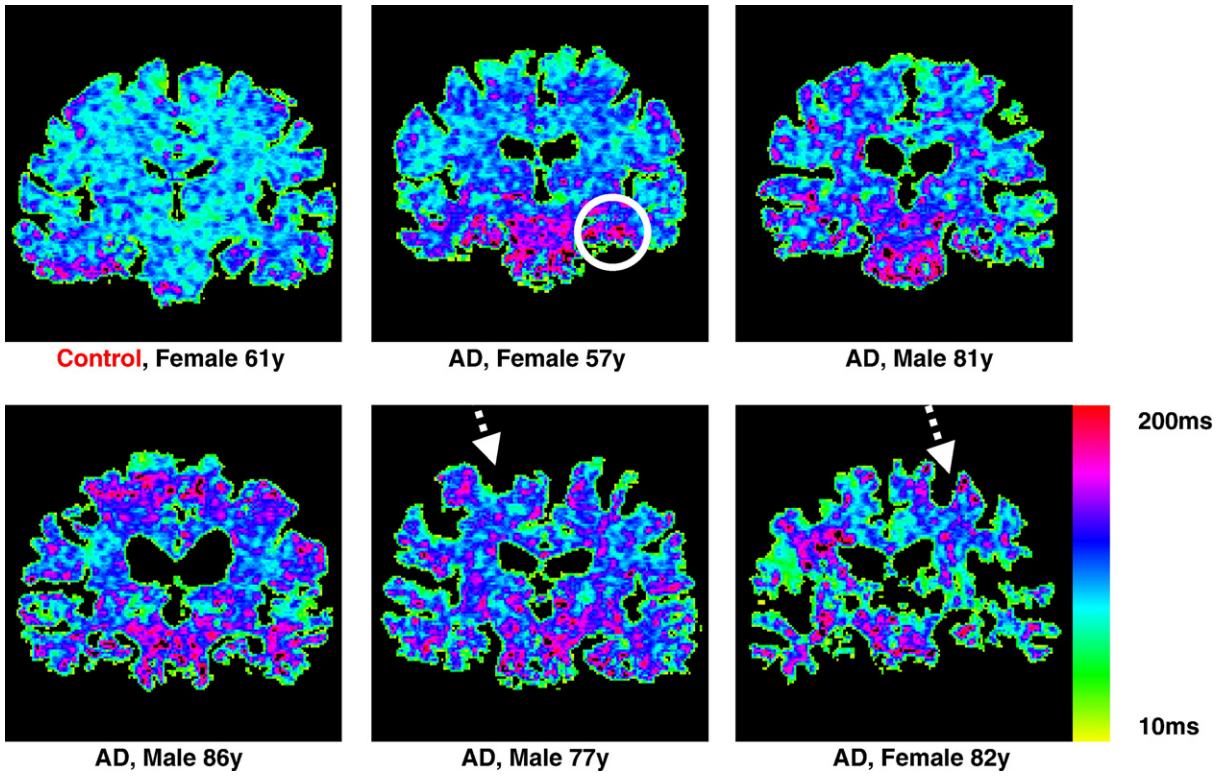

Fig. 3. $T_{1\rho}$ maps obtained in the brains of a control and 5AD patients that were categorized by neurological tests. Color bar on the right ranges from 10 ms to 200 ms with red and magenta colors indicating higher $T_{1\rho}$ values. Pixels with higher $T_{1\rho}$ are more prominent in AD patients especially in the medial temporal lobe region as indicated by the circle on the 57 year-old AD patient. Also noted was increased sulcal space in AD subjects, especially in the older patients (dashed arrows), suggesting greater brain atrophy.

In the fitting routine, pixels whose intensities correlated poorly (i.e. $R^2 < 0.95$) with the fitting equation were set to zero. Pixels outside the brain were also set to zero in the $T_{1\rho}$ color maps. Reproducibility of $T_{1\rho}$ mapping in the human brain was previously measured as coefficients of variation of <2% in the brains of healthy controls (Borthakur et al., 2004) and in AD patients (Borthakur et al., 2006b).

The images were transferred to a G4 PowerBook computer (Apple Corp., Cupertino, CA) and images were processed in custom-written software in the IDL programming language (RSI Corp., Boulder, CO). $T_{1\rho}$ values were automatically reported from the GM and WM in the temporal lobes by an algorithm shown in a flow chart in Fig. 1. Briefly, $T_{1\rho}$ MRI of the same slice of the brain are acquired at four different SL times and employed to generate a $T_{1\rho}$ relaxation time map. Each pixel on the map represents actual $T_{1\rho}$ values (in milliseconds) for that pixel. These maps are typically color-coded for display. GM and WM segmented masks were obtained by segmentation (details in the next section), and an example is shown in the image in the left of center. A program written in IDL was used to automatically record $T_{1\rho}$ values from only pixels that were classified as GM or WM located in either the left or right medial temporal lobe (MTL) region of the brain. The four regions of interest (ROI) are shown in the bottom of the Fig. 1.

Image segmentation

Immediately following $T_{1\rho}$ MRI, the entire volume of each subject's brain was imaged in the coronal plane using a T_1-weighted 3D volumetric MPRAGE MRI sequence with 124 continuous slices, 1.2 mm slice thickness, a FOV of 24 cm and 192 phase-encode steps, and flip angle = 8°.

TE/TR = 3.5 ms/3000 ms for a total imaging time ~10 min. A previously developed and validated (Davatzikos et al., 2008) method (HAMMER) based on a high-dimensional elastic warping of a digital atlas of the human brain (Kabani et al., 2001; Mazziotta et al., 2001) was used to partition an individual's volumetric MRI brain scan into 92 ROIs incorporating all major cortical and sub-cortical structures. These methods deform MRI scans of different brains into anatomical co-registration with each other, and into co-registration with a standardized template. The template's labels are then transferred to the individual scans by applying the elastic transformation that was found to co-register the respective images.

Using this approach, 4 ROIs were defined onto the $T_{1\rho}$ images: left and right temporal lobe WM and GM to automatically report $T_{1\rho}$ values. It is also possible to compare rates of atrophy to $T_{1\rho}$ values in these subjects, however, that analysis is beyond the scope of the work described here.

Table 1
Mean $T_{1\rho}$ (ms) ± standard error of average $T_{1\rho}$ values in all three subject cohorts

Diagnosis	*N*	WM $T_{1\rho}$ mean ± std. err. (ms) *	GM $T_{1\rho}$ mean ± std.err. (ms) **
AD	14	89.7 ± 1.4	90.4 ± 1.1
Control	16	82.8 ± 1.3	86.4 ± 1.1
MCI	11	84.7 ± 1.6	87.6 ± 1.3

* Significant difference ($p < 0.01$) between AD-MCI and AD-control cohorts.
** Significant difference ($p < 0.01$) between AD and control cohorts only. There was no significant difference between MCI-control cohorts for either tissue type.

Statistical analyses

Average $T_{1\rho}$ from both right and left MTL for GM and WM were separately recorded for each subject and recorded in an Excel spreadsheet (Microsoft Corp., Redmond, WA). An analysis of variance (ANOVA) using the JMP statistical package (SAS Inc., Cary, NC) was performed to determine any significant differences between the values obtained in the three volunteer cohorts. The mean and standard error of the average $T_{1\rho}$ values were also determined for both GM and WM in the MTL.

Results

Typical $T_{1\rho}$ images of the brain of a healthy adult with and without fluid-attenuation are shown for comparison (Fig. 2). Note the decreased signal from the sulci and ventricles in image B. Fluid-attenuated $T_{1\rho}$ MRI reduces the likelihood that any elevation in $T_{1\rho}$ relaxation time is due to increased CSF. $T_{1\rho}$ maps from a subset of the test population (Fig. 3) demonstrate a range of $T_{1\rho}$ values in the brains of AD patients, which are typically greater than the controls, as indicated magenta colored pixels. Some AD subjects are also characterized by abnormally large sulcal space (arrows on $T_{1\rho}$ maps of the 77 year-old male and 82 year-old female AD patients). This would suggest that integrating regional atrophy patterns and $T_{1\rho}$ would be a stronger classifier of subjects in to the AD–MCI–controls cohorts. The other AD patients, however, do not necessarily exhibit larger sulcal space but do still possess elevated $T_{1\rho}$. This would indicate early biochemical changes in tissue composition that have not yet manifested in decreased brain volume.

Average $T_{1\rho}$ for GM and WM is listed in Table 1. A statistically significant ($p<0.01$) increase in both the GM and WM in the MTL is seen in AD patients over age-matched controls. However, AD and MCI cohorts only displayed significant difference ($p<0.01$) in WM. There was no significance in the difference in $T_{1\rho}$ between control and MCI cohorts. A possible reason could be the fact that the MCI cohort displays a bi-modal distribution (Fig. 4) with one group having increased $T_{1\rho}$ values in both ROIs while the other group shows no significant increase. While increased $T_{1\rho}$ in GM could indicate AD-related pathology, WM hyper-intensities have been previously reported in T_2-weighted MRI of AD patients (Jefferson et al., 2007). One control patient showed significantly increased $T_{1\rho}$ in both GM and WM. This study will follow these patients for the next 3 years with the further goal of correlating these early $T_{1\rho}$ increases with cognitively normal and MCI patients who develop AD. It is possible that normal aging process may alter relative volume fractions of water and protein in brain tissue and this will be reflected as changes in $T_{1\rho}$ relaxation time. Therefore, we investigated whether $T_{1\rho}$ displays any trend with age. Fig. 5, however, dispels any such expectations, as we did not observe any trend in $T_{1\rho}$ in both GM and WM with age in all subjects. This would suggest that the discrimination of the cohorts based on $T_{1\rho}$ is due to an underlying pathology related to AD other than normal age-related changes in the brain.

Discussion

Evaluation of potential new therapies and longitudinal monitoring of disease progression requires objective and quantitative imaging strategies sensitive to early biochemical changes in brain tissue. The results presented here show that $T_{1\rho}$ MRI is increased by 6% in the AD cohort compared to controls. Both the normal controls and the MCI individuals displayed a somewhat bi-modal distribution in the WM $T_{1\rho}$ signal (albeit the sample size if to small to draw any conclusions). Follow-up studies will allow one to examine whether the normal and MCI individuals with high values are the ones that progress to AD or not. However, there is ample evidence in the literature to suggest that a significant number of cognitive normal elderly, and the majority of MCI individuals, have quite pronounced AD pathology. Recently developed high-dimensional pattern classification methods (Davatzikos et al., 2008) have also shown that distinctive patterns of atrophy are present in those groups. Therefore, it is possible that the individuals with AD-like $T_{1\rho}$ levels do actually have significant amounts of plaques and tangles. Histo-pathological validation is beyond the scope of the present study.

Although there is abundant literature on studies of T_1 and T_2 relaxation times in biological systems, there are relatively few studies

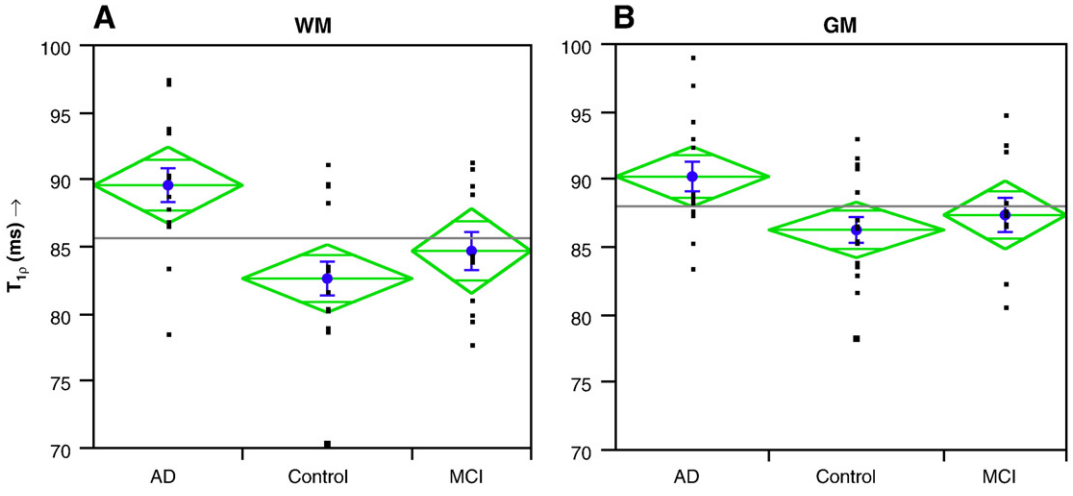

Fig. 4. Average (±std. error, indicated as blue bars) of $T_{1\rho}$ in the AD, control, and MCI cohorts in WM (A) and GM (B) of the MTL. An 8% increase in $T_{1\rho}$ was present in AD over control in the WM ($p<0.01$), while only a 5% increase in $T_{1\rho}$ ($p<0.05$) was observed in GM. The MCI cohort's average $T_{1\rho}$ values were between the AD and control cohorts. Also displayed are the 95% confidence limits (top and bottom apex of each diamond) and 95% overlap marks (horizontal lines within each diamond).

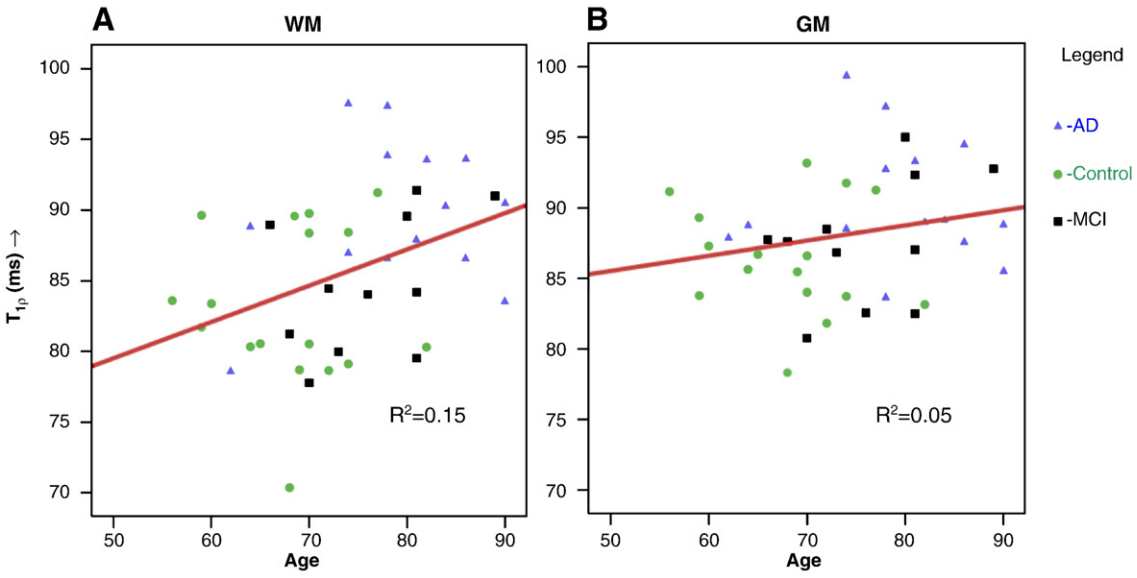

Fig. 5. Plot of $T_{1\rho}$ in GM (A) and WM (B) with age of the subject. No significant correlation was observed in either tissue type (R^2 = 0.15 and 0.04, respectively) with age.

on $T_{1\rho}$ mechanisms in biological tissues. In biological tissues, the $T_{1\rho}$ relaxation could have contributions from several MR interactions such as chemical exchange, dipolar interaction, J-coupling, etc. Depending upon the tissue type, more than one mechanism may be operative simultaneously but with different relative contributions.

$T_{1\rho}$ experiments have the potential to provide information about the low frequency motions (100 Hz to a few kHz) in biological systems. For example, protons exchanging between free water and those in a "bound" state (due to their proximity to proteins) occur in the timescale of a few milliseconds. These protons would preferentially contribute to $T_{1\rho}$ MR signal when spin-locked at amplitudes of 500 Hz. For this reason, it is possible for $T_{1\rho}$ MRI to probe protein content in an indirect manner in tissues such as cartilage, brain and blood.

Implementing this research sequence into a clinical imaging protocol requires a few modifications. For instance, a 3D volumetric coverage of the entire brain has to be provided with high signal and temporal efficiency but without exceeding RF energy deposition limits, measured as SAR. Since $T_{1\rho}$ mapping involves collection of at least four 3D data sets at varying SL times, it is inherently inefficient. To overcome this limitation of the current imaging protocol, we recently incorporated $T_{1\rho}$ imaging with a balanced steady-state free precession (b-SSFP) sequence (Witschey et al., in press). The performance of this new pulse sequence, named SLIPS, was verified by comparing $T_{1\rho}$ relaxation maps with that of the single-slice $T_{1\rho}$-TSE sequence used in the current experiments. The average difference in $T_{1\rho}$ was less than 5% in $T_{1\rho}$ maps of the same brain, while the imaging time for a SLIPS-acquired 3D data set of 16 slices was only 2 min, indicating a total imaging time of less than 10 min for all four 3D data sets. Integrating SLIPS with parallel imaging techniques using a multi-channel head coil is expected to further reduce imaging time. Additionally, a low SAR version of $T_{1\rho}$ mapping sequence was developed by our group (Wheaton et al., 2004). This method exploits a partial k-space acquisition approach in which a full power spin-lock pulse is applied only to the central phase-encode lines of k-space, while the remaining phase-encode lines receive a low-power (50% amplitude of the maximum) spin-lock pulse. Acquisition of high- and low-power phase-encode lines are interleaved temporally to minimize average power deposition. This strategy ensured that the majority of signal energy in the central portion of k-space was fully $T_{1\rho}$ weighted, while at the same time the overall SAR of the acquisition was lower, and consequently, total imaging time was reduced. It was demonstrated that using this approach in the human brain that SAR could be reduced by 40% while the measurements of $T_{1\rho}$ changed by only 2%. Similarly, a "keyhole" acquisition approach was exploited in reducing the overall imaging time by 40% for $T_{1\rho}$ mapping (Wheaton et al., 2003). These approaches can be combined with any of the acquisition sequences described above to reduce SAR and/or improve temporal resolution.

The long-term goals will be to extend this study in the following directions: longer follow-up and additional treatment modalities (e.g., rehabilitation, novel therapies, etc.), and basic science study of AD pathology.

Disclosure statement for authors

No conflicts of interest.

Acknowledgments

This work was performed at a NIH supported resource center (NIH RR02305) and from a grant from the Pennsylvania State Tobacco Settlement. We thank Professor Ravinder Reddy for his thoughtful comments and funding support.

References

Aronen, H.J., Ramadan, U.A., et al., 1999. 3D spin-lock imaging of human gliomas. Magn. Reson. Imaging 17 (7), 1001–1010.

Benveniste, H., Einstein, G., et al., 1999. Detection of neuritic plaques in Alzheimer's disease by magnetic resonance microscopy. Proc. Natl. Acad. Sci. U. S. A. 96 (24), 14079–14084.

Borthakur, A., Wheaton, A.J., et al., 2004. In vivo measurement of T1rho dispersion in the human brain at 1.5 tesla. J. Magn. Reson. Imaging 19 (4), 403–409.

Borthakur, A., Gur, T., et al., 2006a. In vivo Measurement of Plaque Burden in a Mouse Model of Alzheimer's Disease. J. Magn. Reson. Imaging 24 (5), 1011–1017.

Borthakur, A., Moonis, G., et al., 2006b. Fluid-attenuated T1rho of the human brain in vivo. Proceedings of the International Society of Magnetic Resonance in Medicine, 14th Scientific Meeting. ISMRM, Seattle.

Chetelat, G., Baron, J.C., 2003. Early diagnosis of Alzheimer's disease: contribution of structural neuroimaging. NeuroImage 18 (2), 525–541.

Convit, A., De Leon, M.J., et al., 1997. Specific hippocampal volume reductions in individuals at risk for Alzheimer's disease. Neurobiol. Aging 18 (2), 131–138.

Cook, M.J., Fish, D.R., et al., 1992. Hippocampal volumetric and morphometric studies in frontal and temporal lobe epilepsy. Brain 115 (Pt 4), 1001–1015.

Davatzikos, C., Genc, A., et al., 2001. Voxel-based morphometry using the RAVENS maps: methods and validation using simulated longitudinal atrophy. NeuroImage 14, 1361–1369.

Davatzikos, C., Fan, Y., et al., 2008. Detection of prodromal Alzheimer's disease via pattern classification of magnetic resonance imaging. Neurobiol. Aging 29 (4), 514–523.

Dawbarn, D., Allen, S.J., 2001. Neurobiology of alzheimer's disease. Oxford University Press, New York.

de Leon, M.J., DeSanti, S., et al., 2006. Longitudinal CSF and MRI biomarkers improve the diagnosis of mild cognitive impairment. Neurobiol. Aging 27 (3), 394–401.

De Santi, S., de Leon, M.J., et al., 2001. Hippocampal formation glucose metabolism and volume losses in MCI and AD. Neurobiol. Aging 22 (4), 529–539.

DeCarli, C., Kaye, J.A., et al., 1990. Critical analysis of the use of computer-assisted transverse axial tomography to study human brain in aging and dementia of the Alzheimer type. Neurology 40 (6), 872–883.

Dixon, W.T., Oshinski, J.N., et al., 1996. Myocardial suppression *in vivo* by spin locking with composite pulses. Magn. Reson. Med. 36 (1), 90–94.

Gonzalez, R.G., Fischman, A.J., et al., 1995. Functional MR in the evaluation of dementia: correlation of abnormal dynamic cerebral blood volume measurements with changes in cerebral metabolism on positron emission tomography with fludeoxyglucose F 18. Am. J. Neuroradiol. 16 (9), 1763–1770.

Hampel, H., Teipel, S.J., et al., 2002. Age transformation of combined hippocampus and amygdala volume improves diagnostic accuracy in Alzheimer's disease. J. Neurol. Sci. 194 (1), 15–19.

Helpern, J.A., Lee, S.P., et al., 2004. MRI assessment of neuropathology in a transgenic mouse model of Alzheimer's disease. Magn. Reson. Med. 51 (4), 794–798.

Jack Jr., C.R., Petersen, R.C., et al., 1999. Prediction of AD with MRI-based hippocampal volume in mild cognitive impairment. Neurology 52 (7), 1397–1403.

Jack Jr., C.R., Shiung, M.M., et al., 2004. Comparison of different MRI brain atrophy rate measures with clinical disease progression in AD. Neurology 62 (4), 591–600.

Jefferson, A.L., Massaro, J.M., et al., 2007. Inflammatory biomarkers are associated with total brain volume: the Framingham Heart Study. Neurology 68 (13), 1032–1038.

Kabani, N., Le Goualher, G., et al., 2001. Measurement of cortical thickness using an automated 3-D algorithm: a validation study. NeuroImage 13 (2), 375–380.

Lee, V.M., Goedert, M., et al., 2001. Neurodegenerative tauopathies. Annu. Rev., Neurosci. 24, 1121–1159.

Markkola, A.T., Aronen, H.J., et al., 1998. Determination of T1rho values for head and neck tissues at 0.1 T: a comparison to T1 and T2 relaxation times. Magn. Reson. Imaging 16 (4), 377–383.

Mazziotta, J., Toga, A., et al., 2001. A four-dimensional probabilistic atlas of the human brain. J Am. Med. Inform Assoc. 8 (5), 401–430.

McDaniel, B., Sheng, H., et al., 2001. Tracking brain volume changes in C57BL/6J and ApoE-deficient mice in a model of neurodegeneration: a 5-week longitudinal micro-MRI study. NeuroImage 14 (6), 1244–1255.

Moseley, M.E., deCrespigny, A., et al., 1996. Magnetic resonance imaging of human brain function. Surg. Neurol. 45 (4), 385–391.

Pfefferbaum, A., Mathalon, D.H., et al., 1994. A quantitative magnetic resonance imaging study of changes in brain morphology from infancy to late adulthood. Arch. Neurol. 51 (9), 874–887.

Sandor, T., Jolesz, F., et al., 1992. Comparative analysis of computed tomographic and magnetic resonance imaging scans in Alzheimer patients and controls. Arch. Neurol. 49 (4), 381–384.

Santyr, G.E., 1994. MR imaging of the breast Imaging and tissue characterization without intravenous contrast. Magn. Reson. Imaging Clin. N. Am. 2 (4), 673–690.

Selkoe, D.J., 1999. Translating cell biology into therapeutic advances in Alzheimer's disease. Nature 399 (6738 Suppl), A23–A31.

Shen, D., Davatzikos, C., 2002. HAMMER: hierarchical attribute matching mechanism for elastic registration. IEEE. Trans. Med. Imag. 21 (11), 1421–1439.

Sullivan, E.V., Shear, P.K., et al., 1993. Greater abnormalities of brain cerebrospinal fluid volumes in younger than in older patients with Alzheimer's disease. Arch. Neurol. 50 (4), 359–373.

Thompson, P.M., Hayashi, K.M., et al., 2007. Tracking Alzheimer's disease. Ann. N. Y. Acad. Sci. 1097, 183–214.

Uryu, K., Laurer, H., et al., 2002. Repetitive mild brain trauma accelerates Abeta deposition, lipid peroxidation, and cognitive impairment in a transgenic mouse model of Alzheimer amyloidosis. J. Neurosci. 22 (2), 446–454.

Wheaton, A.J., Borthakur, A., et al., 2003. Application of the keyhole technique to T1rho relaxation mapping. J. Magn. Reson. Imag. 18 (6), 745–749.

Wheaton, A.J., Borthakur, A., et al., 2004. Method for reduced SAR T1rho-weighted MRI. Magn. Reson. Med. 51 (6), 1096–1102.

Witschey, W.R., Borthakur, A. et al., in press. T1rho-Prepared Balanced Steady-State Free Precession for Rapid 3D T1rho-weighted MRI. J. Magn. Reson. Imag.